Journal of Fluids and Structures (2000) **14,** 429–440
doi:10.1006/jfls.1999.0278, available online at http://www.idealibrary.com on IDEAL®

DNS-DERIVED FORCE DISTRIBUTION ON FLEXIBLE CYLINDERS SUBJECT TO VORTEX-INDUCED VIBRATION

C. Evangelinos, D. Lucor and G. E. Karniadakis*
Center for Fluid Mechanics, Division of Applied Mathematics, Brown University Providence, RI 02912, U.S.A.

(Received 15 March 1999, and in final form 9 November 1999)

We use direct numerical simulation (DNS) based on spectral methods to simulate turbulent flow past rigid and flexible cylinders subject to vortex-induced vibrations (VIV). We present comparisons of amplitude, and lift and drag forces, at Reynolds number 1000 for a short and a long cylinder, and we examine differences between a traveling wave response and a standing wave response. The DNS data suggest that the often-used empirical formula proposed by Skop, Griffin & Ramberg in 1977 overpredicts the drag coefficient. We propose an appropriate modification and present preliminary results that indicate that low-dimensional modeling may be an accurate and efficient approach in predicting forces in VIV. Given the lack of any benchmark experiments in VIV currently, the DNS results presented here, both distributions as well as span- and time-averaged quantities, should be helpful to experimentalists and modelers.

1. INTRODUCTION

The prediction of vortex-induced vibrations (VIV) is currently based on semi-empirical methods, all of which depend on the values of drag and lift coefficients, either the sectional values or the span-averaged values [see, for example, Blevins (1990), Naudascher & Rockwell (1993), Parkinson (1989)]. Despite the extensive force measurements for the *rigid* cylinder undergoing forced or free transverse vibrations (Sarpkaya 1978; Staubli 1983; Gopalkrishnan 1993; Khalak & Williamson 1997; Hover *et al.* 1998) considerably less is known for the flexible cylinder subject to VIV [see Alexander (1981), Yoerger *et al.* (1991), Vandiver (1983)]. In particular, we are not aware of any direct measurements for lift, drag and amplitude for either the rigid or flexible cylinder, with the exception of the recent work by Khalak & Williamson (1997) for a freely vibrating rigid cylinder.

In addition to this lack of benchmark experiments, a survey of the relevant literature reveals very large variations in the reported values of both the lift and drag coefficients of the order of 100% or more. For example, Vandiver (1983) measured a drag coefficient for a cable in the range of 1·6–3·5 whereas Kim *et al.* (1985) obtained values of C_d from 1·4 to 1·6 for cables 10 times longer than in Vandiver's experiment (Vandiver 1983). Yoerger *et al.* (1991) obtained a value of C_d in the range of 2·2–2·5 for long cables. In contrast, Alexander (1981) obtained an almost constant value of about $C_d \approx 1{\cdot}8$ in experiments with long flexible cylinders. Although this variation is, in most cases, due to different experimental conditions, even in cases with relatively similar conditions, substantial variations in the lift, drag, and cylinder displacement have been reported. It is clear that, in such a complex dynamic phenomenon as VIV, even a small variation in the many parameters of the system,

0889–9746/00/040429 + 12 $35.00/0

i.e., mass ratio, bending stiffness, cylinder length, may lead to substantial changes in the response.

In the absence of any benchmark experiments and with the recent success in simulating accurately VIV without any *ad hoc* flow modeling [see Newman & Karniadakis (1997), Evangelinos & Karniadakis (1999)], we address in this paper the aforementioned differences using spectral direct numerical simulation (DNS). Specifically, we consider free transverse oscillations of a flexible cylinder subject to VIV at Reynolds number Re = 1000 corresponding to a turbulent wake. We investigate both short and long cylinders corresponding to length-to-diameter ratio of 4π and 378, respectively. We also examine differences due to a standing wave response versus a traveling wave response, the latter being more typical for longer cylinders (Alexander 1981).

Our objective in this paper is to provide details of the force distribution and the main factors that affect them in a simplified setting but one that resembles closely VIV experiments. Elucidation of the physics and understanding of flow patterns has been presented elsewhere (Evangelinos & Karniadakis 1999).

2. PARAMETERS IN DIRECT NUMERICAL SIMULATION

We report here simulation results at Reynolds number Re = 1000 and mass ratio (nondimensionalized cylinder linear density) $\rho = 2$, which is a typical value for VIV in water. The Reynolds number is defined based on the cylinder diameter d and the free-stream velocity U. In all cases we neglect the structural damping as we are interested in the maximum amplitude response. We also allow only vertical motions in the crossflow y-direction, i.e., we do not allow any motion in the streamwise x-direction. We have chosen the structure eigenfrequency Ω to be equal to the Strouhal number of the corresponding stationary cylinder flow as we are interested in lock-in states only. Deviations from this resonant state and transition to quasi-periodic states have also been studied by Evangelinos (1999).

The governing equations are the incompressible Navier–Stokes equations coupled with the equation of the structure dynamics. In the following analysis, all quantities (unless explicitly stated) are assumed to be nondimensionalized with respect to the cylinder diameter d and the free-stream velocity U. We will refer to a *beam* as the structure whose dynamics is described by

$$\frac{\partial^2 y}{\partial t^2} = -\gamma^2 \frac{\partial^4 y}{\partial z^4} + \frac{F}{\rho} \tag{1}$$

in a simplified linear setting, with motion constrained to be in the y–direction and in the absence of damping. Here, $\gamma^2 = EI/\rho$ with EI the bending stiffness. Also, F is the total lift force, i.e., the sum of pressure and viscous forces exerted by the fluid to the structure in the y-direction.

Equation (1) reduces to a forced harmonic oscillator in Fourier space. Employing a Fourier series representation

$$\frac{\mathrm{d}^2 \hat{y}_m}{\mathrm{d}t^2} = -\Omega_n^2 m^4 \hat{y}_m + \frac{\hat{F}_m}{\rho}, \tag{2}$$

with $\hat{y}_m(t)$ the amplitude of the mth structural mode of vibration and $\hat{F}_m(t)$ the projection of the external lift force to the same mode. Depending on the choice of boundary conditions, we use either a (complex exponential) Fourier series in terms of $\mathrm{e}^{2\mathrm{i}m\pi z/L_z}$ (for the case of a beam with freely moving periodic end-points) or a Fourier sine series in terms of

$\sin(m\pi z/L_z)$ (for the case of a beam with pinned end-points). The length of the beam in the equilibrium position is L_z. The sine series representation naturally satisfies the condition $y = \partial^2 y/\partial z^2 = 0$ at the end-points of the beam. A Fourier series representation gives

$$\Omega_n = \gamma(2\pi/L_z)^2, \tag{3}$$

while a Fourier sine series gives

$$\Omega_n = \gamma(\pi/L_z)^2. \tag{4}$$

To establish lock-in for the structural mode m we choose

$$\Omega = \Omega_n m^2 \approx 2\pi\mathrm{St}, \tag{5}$$

where St is the Strouhal number of the corresponding stationary cylinder flow. We are interested in the first mode $m = 1$ for the case of the free periodic boundary conditions. This mode in the Fourier series representation would be the second mode $m = 2$. Employing equations (5) and (3) at $m = 1$ leads to

$$\gamma \approx \frac{1}{2}\frac{L_z^2}{\pi}\,\mathrm{St} \Rightarrow EI \approx \frac{1}{4}\,\rho\,\frac{L_z^4}{\pi^2}\,\mathrm{St}^2. \tag{6}$$

Employing equations (5) and (4) at $m = 2$ reduces again to expression (6), because of the m^2 term in equation (5).

We performed simulations with two different values of the spanwise length, i.e., $L_z = 4\pi$ and 378. We also performed simulations with the ends of the cylinder *free* or *fixed (pinned)* at zero displacement. This is accomplished by projecting the force F into a Fourier sine series that gives zero contributions at the two ends.

The coupled Navier–Stokes/structure dynamics equations are discretized in space using a new spectral method that employs a hybrid grid in the x–y plane and Fourier complex modes in the z-direction (cylinder axis). The parallel code $\mathcal{N}\varepsilon\kappa\tau\alpha\rho$ written in $C{+}{+}$ and MPI is employed in all simulations (Warburton 1998). A boundary-fitted coordinate system is employed, similar to the laminar flow simulations of Newman & Karniadakis (1997), which has been validated against an arbitrary Lagrangian Euler (ALE) formulation we have also developed for moving domains (Warburton & Karniadakis 1997). More details about the numerical method and the discretization employed in the current simulations can be found in Evangelinos (1999).

3. SPATIO-TEMPORAL VARIATION OF AMPLITUDE, LIFT AND DRAG

It has been shown by Bloor (1964) for a stationary cylinder and also confirmed numerically by Evangelinos & Karniadakis (1999) that the flow past a stationary cylinder, as well as the flow past transversely oscillating cylinders, is turbulent at $\mathrm{Re} = 1000$. This has been documented by the velocity spectra of the near wake that show clearly an inertial range of about half a decade in wave number. In the following, we perform systematic simulations at that Reynolds number as higher Reynolds number simulations are prohibitively expensive. We will first present distribution of forces along the span and in time, and subsequently we will compare span-averaged and time-averaged quantities.

3.1. VIV of Rigid Cylinders

First, we present results from simulations of flow past a *rigid* cylinder at $\mathrm{Re} = 1000$ subject to VIV. The spanwise length is $L_z = 4\pi$ and periodic boundary conditions are imposed at

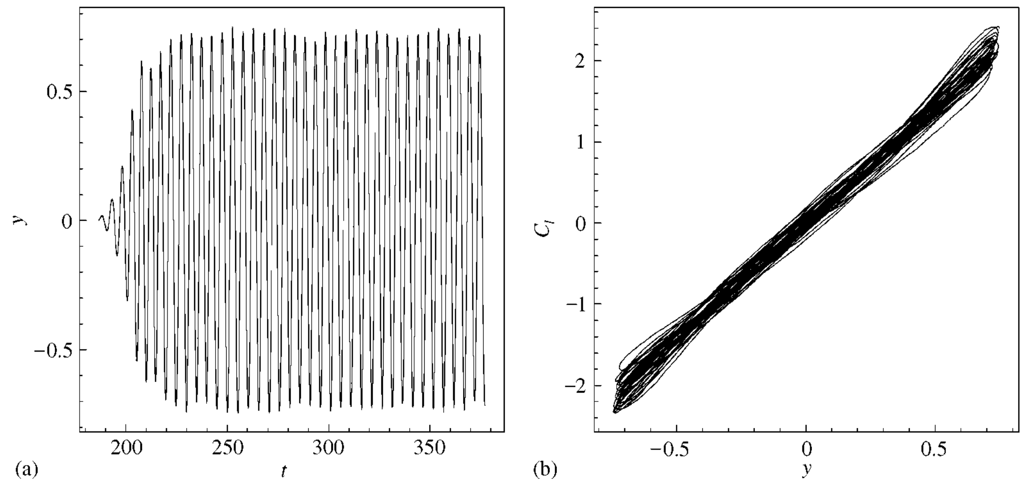

Figure 1. Rigid cylinder: (a) cross-flow (nondimensional) displacement versus (nondimensional) time; (b) span-averaged lift coefficient versus cross-flow displacement.

the two ends along the cylinder axis. We see in Figure 1(a) that a slightly modulated harmonic motion is produced with maximum amplitude $y_{\max} \approx 0{\cdot}75$, which is larger than the corresponding value of the two-dimensional simulation of $y_{\max} \approx 0{\cdot}55$. This motion is *in-phase* with the span-averaged lift coefficient as revealed in the phase portrait shown in Figure 1(b), in agreement with the experiments of Brika & Laneville (1993). The rigid cylinder is allowed to oscillate only in the cross-flow direction, and therefore the motion is uniform along its axis. However, the corresponding flow is strongly three dimensional, as shown by the spanwise distribution of lift coefficient in Figure 2. It exhibits strong cellular structure, with peaks exceeding values of the span-averaged coefficient by almost 50%. The same cellular structure in the span-time domain is present in the drag coefficient [see lower plot in Figure 2, as well as the energy exchange between the cylinder and the flow in Evangelinos (1999)].

The lock-in state of the freely oscillating rigid cylinder corresponds to a two-branch response as it was documented in the detailed experiments of Khalak & Williamson (1996). The upper branch corresponds to large amplitude and low values of reduced velocity, and the lower branch corresponds to low amplitudes and large values of the reduced velocity. A similar result was also obtained by Hover *et al.* (1998) at a Reynolds number Re $= 3800$, which is lower than in Khalak & Williamson (1996) but at comparable (small) values of the structural damping. The classical results of Feng (1968) were obtained for relatively large damping [see also Brika & Laneville (1993)] but essentially show the same response at reduced levels. By comparing the numerical results here with both sets of recent experiments, it is clear that the three-dimensional simulations capture the upper branch corresponding to an oscillation *in-phase* with the lift coefficient. There is also agreement in the amplitude of oscillation with the experimental data, especially with the data of Hover *et al.* (1998), which were obtained at Re $= 3800$, closer to the Reynolds number in our simulation.

3.2. VIV of Flexible Beams

We simulate four different cases of turbulent flow past a flexible beam, in order to investigate both the effect of the aspect ratio of the beam as well as the effect of the boundary conditions in the spanwise direction. Specifically, we consider both *periodic ends* (Case A) as well as *fixed ends* (Case B); with subscripts (s) and (l) we will denote the short beam ($L_z = 4\pi$) and long beam ($L_z = 378$), respectively. Regarding initial conditions, for the short beam for Case A_s, we start by prescribing a standing wave as the initial state. For Case B_s we start from simulation results of a stationary cylinder at $Re = 1000$. For the long beam we interpolated results from the shorter beam by increasing the cylinder length gradually from $L_z = 4\pi$ to $= 378$ for Case A_l. For the fixed ends (Case B_l) we used results from the periodic ends Case (A_l) as initial conditions.

In Figure 3 we plot the cross-flow displacement of the short beam for both boundary conditions versus time. For Case A_s, a transition from the initially prescribed standing wave to a modulated traveling wave response takes place; only the asymptotic stable traveling response is plotted in the figure. For Case B_s, we also plot the asymptotic stable standing wave response, and we see that the maximum amplitude is more than one cylinder diameter, and in fact about 20% higher than the traveling wave response. In Figure 4 we plot the cross-flow displacement of the long beam for both boundary conditions versus time. We see that the response is similar as in the short beam case but the amplitude of vibration is reduced. Moreover, there seems to be a substantial motion of the middle "node" for the standing wave response, as instantaneously more than one node exist around the mid-span, in contrast to the response of the short beam. This result is in agreement with experimental results as well as field data (Furnes 1998).

In Figure 5, we plot the lift coefficient of the short beam. We see that, for Case A_s, the maximum lift coefficient is subject to very large modulation following the large variation in phase difference, unlike the freely oscillating rigid cylinder. For example, regions of small phase difference (less than 10°) result in values of maximum lift coefficient of more than $C_l \approx 2$, but phase differences of 90° or higher are also possible leading to lift coefficient amplitudes of less than $C_l \approx 0{\cdot}5$. For Case B_s, the lift variation is also large but it follows the standing wave response. The same cellular patterns are present in the long beam but with the maximum values of the lift coefficient quite larger compared to the values for the shorter beam. Specifically, for Case A_l, we obtained $C_l \approx \pm 3$ and, for Case B_l, we obtained $C_l \approx \pm 3{\cdot}5$.

In Figure 6 we plot the drag coefficient for the short beam. Very large values of the drag coefficient are obtained locally for both boundary conditions. These values are about three times higher than the drag coefficient for a stationary cylinder. The same is true for the long beam. Specifically, the maximum value for C_d is approximately 3·4 and 4·0 for Cases A_l and B_l, respectively. Similarly, the minimum value of C_d is approximately 0·7 (Case A_l) and 0·55 (Case B_l).

4. COMPARISON OF TIME-AVERAGED AND SPAN-AVERAGED FORCES

In Figure 7, we plot the standard deviation of the motion of the beam with fixed ends along its axis for the short and long beam. We also include for reference the corresponding values for the rigid cylinder and the traveling wave response obtained for similar conditions. We see that for the short beam the traveling wave response is very close to the oscillating rigid cylinder, although the former corresponds to larger values of maximum amplitude. Note that the motion of the node is nonzero as there is some small movement of the node, which is more pronounced especially for the long beam. Also, the displacement of the long beam is lower than the short beam and similar behavior has been reported by Alexander (1981). This difference may also be due to the relatively lower resolution along the span employed in the longer beam, but this could not be quantified at the present time. It is clear, however, that the smaller flow scales cannot be resolved sufficiently since for the long beam the grid spacing is about $6d$ in that case as compared to $0{\cdot}2d$ in the short beam.

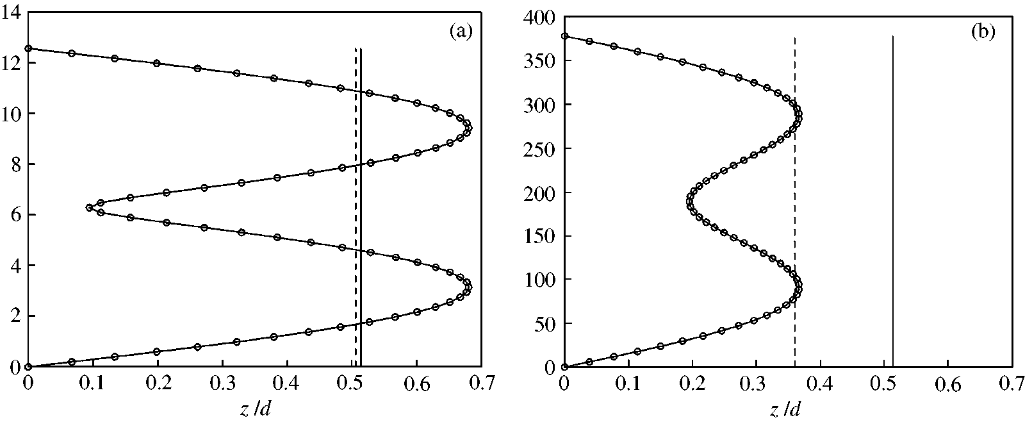

Figure 7. Standard deviation of the displacement along the span for (a) a short beam and (b) a long beam. The solid line is the rigid line response and the dashed line is the traveling wave response.

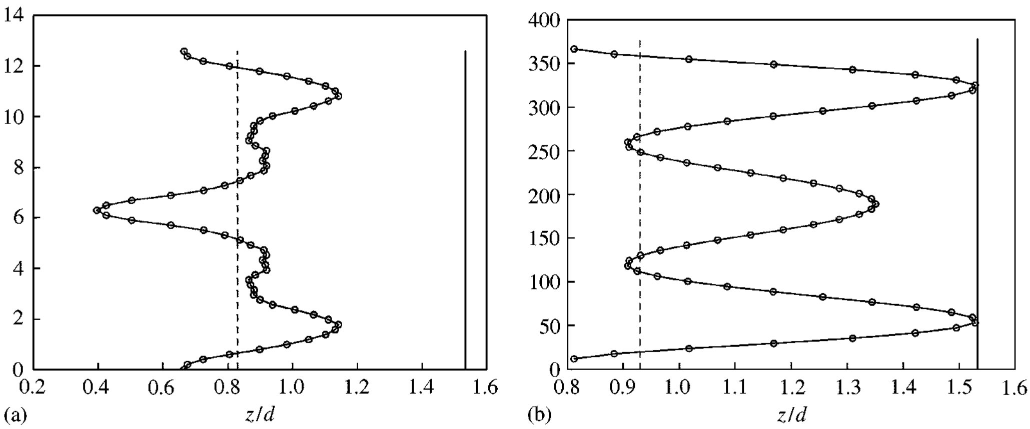

Figure 8. Standard deviation of the lift coefficient along the beam for (a) a short beam and (b) a long beam. The solid line is the rigid line response and the dashed line is the traveling wave response.

In Figure 8 we plot the standard deviation of the lift coefficient of the beam with fixed ends along its axis for the short and long beam. We also include for reference the corresponding values for the rigid cylinder and the traveling wave response. We see that the span-averaged value is about the same for Cases A_s and B_s, and similarly for the long beam. The value for the rigid cylinder is substantially larger compared to all cases simulated.

In Figures 9 and 10, we plot the mean and standard deviation of the drag coefficient of the beam with fixed ends along its axis for the short and long beam. We also include for reference the corresponding values for the rigid cylinder and the traveling wave response. We see that the mean drag coefficient for all cases is in the range of 1·6–1·8, in agreement with the experiments of Alexander (1981), except for the rigid cylinder that corresponds to a mean drag coefficient of approximately 2·1. The r.m.s. values of the drag coefficient for the oscillating rigid cylinder are more than 30 times larger than the values of the stationary cylinders, in agreement with the findings of Khalak & Williamson (1997).

We now turn our attention to time variation of the span-averaged quantities. In particular, we are examining the cases where homogeneity exists along the spanwise

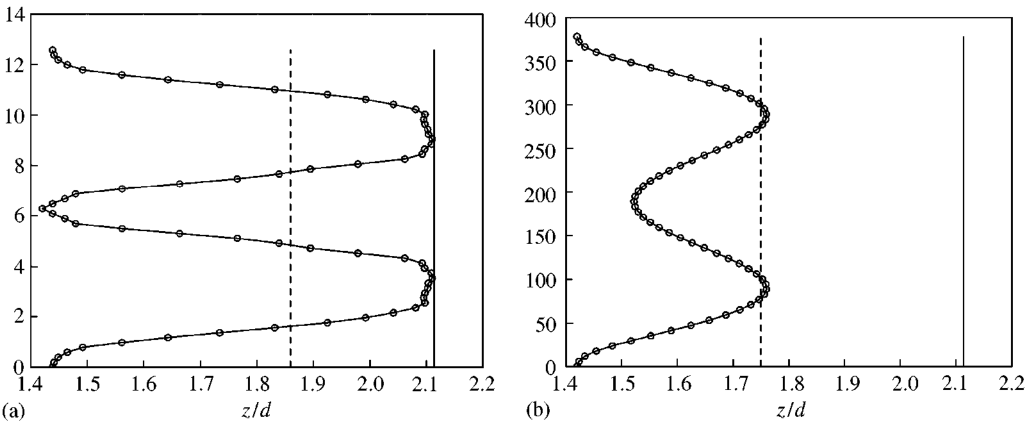

Figure 9. Variation of the mean drag coefficient along the beam for (a) a short beam and (b) a long beam. The solid line is the rigid line response and the dashed line is the traveling wave response.

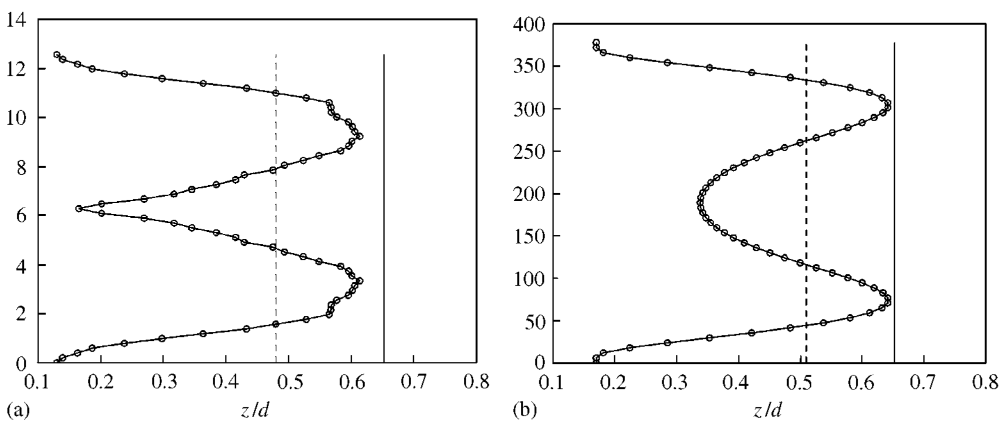

Figure 10. Standard deviation of the drag coefficient along the beam for (a) a short beam and (b) a long beam.

direction, which is not true, for example, for the fixed ends cases. To summarize the results regarding the cylinder lift forces, we plot in Figure 11 the histories of span-averaged lift coefficient for the rigid freely oscillating cylinder, and the short and long beam. We also include for reference the corresponding values of the coefficients for a stationary cylinder subject to uniform flow at Re $=$ 1000. We see that the lift coefficient of the freely oscillating rigid cylinder is much larger than all the other cases, and that the stationary cylinder has the smallest mean and r.m.s. values. Measurements of the lift forces for the rigid cylinder corresponding to very *small structural damping* have been performed only recently by Khalak & Williamson (1997) and by Hover *et al.* (1998). It was found that very large values of the lift coefficient are possible at lock-in, close to the values observed in the simulations, although the experimental values are somewhat higher, especially in the experiments of Khalak & Williamson (1997), possibly due to the higher Reynolds number.

To summarize the results regarding the cylinder drag forces, we plot in Figure 12 the histories of span-averaged drag coefficient for the rigid freely oscillating cylinder, and the short and long beam along with the history for a stationary cylinder. Here we can see the very large amplitudes of the drag coefficient compared to the stationary cylinder. Using the DNS data, for example the more accurate data for the short beam, we can also evaluate

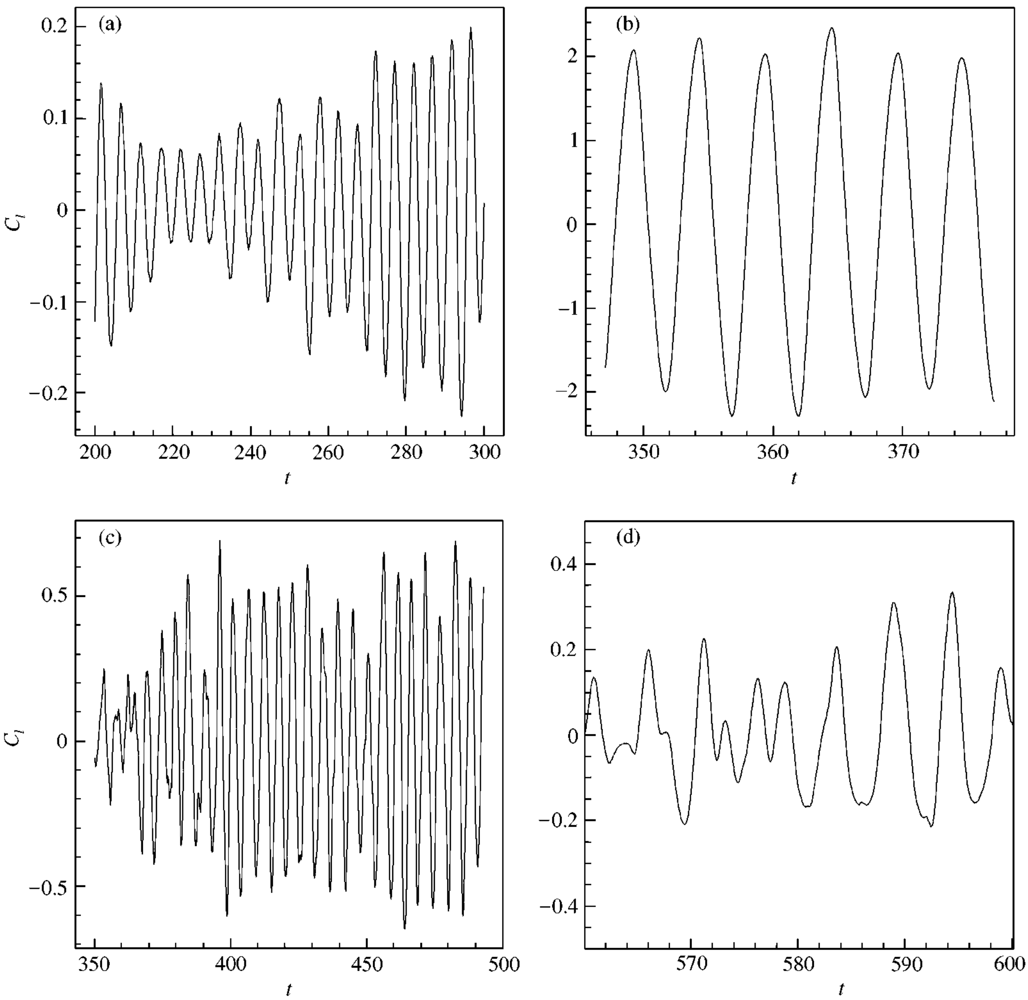

Figure 11. Comparison of span-averaged lift coefficient histories for (a) a stationary cylinder, (b) a freely oscillating rigid cylinder, (c) a short beam with free ends, and (d) a long beam with free ends.

the empirical formula due to Skop *et al.* (1977),

$$C_d = C_{d0}\left[1 + 1{\cdot}043\left(\frac{2y_{\mathrm{r.m.s.}}}{d}\right)^{0{\cdot}65}\right], \tag{7}$$

where $C_{d0} = 1{\cdot}04$ is the drag coefficient of a stationary cylinder, $y_{\mathrm{r.m.s}}$ is the r.m.s. amplitude of the motion, and d is the cylinder diameter. In Figure 13 we plot the prediction from the above equation using the r.m.s. amplitude values for the short beam (see Figure 7) against the DNS data. We see that equation (7) overpredicts the DNS data. Instead, a better approximation is given by

$$C_d = C_{d1}\left[1 + A\left(\frac{2y_{\mathrm{r.m.s.}}}{d}\right)^{B}\right], \tag{8}$$

where $A = 0{\cdot}355$ and $B = 0{\cdot}9$ (shown also in the Figure marked with diamonds). Note that C_{d1} is here the drag coefficient at the nodes which is about 1·4. Equation (8) is very similar to

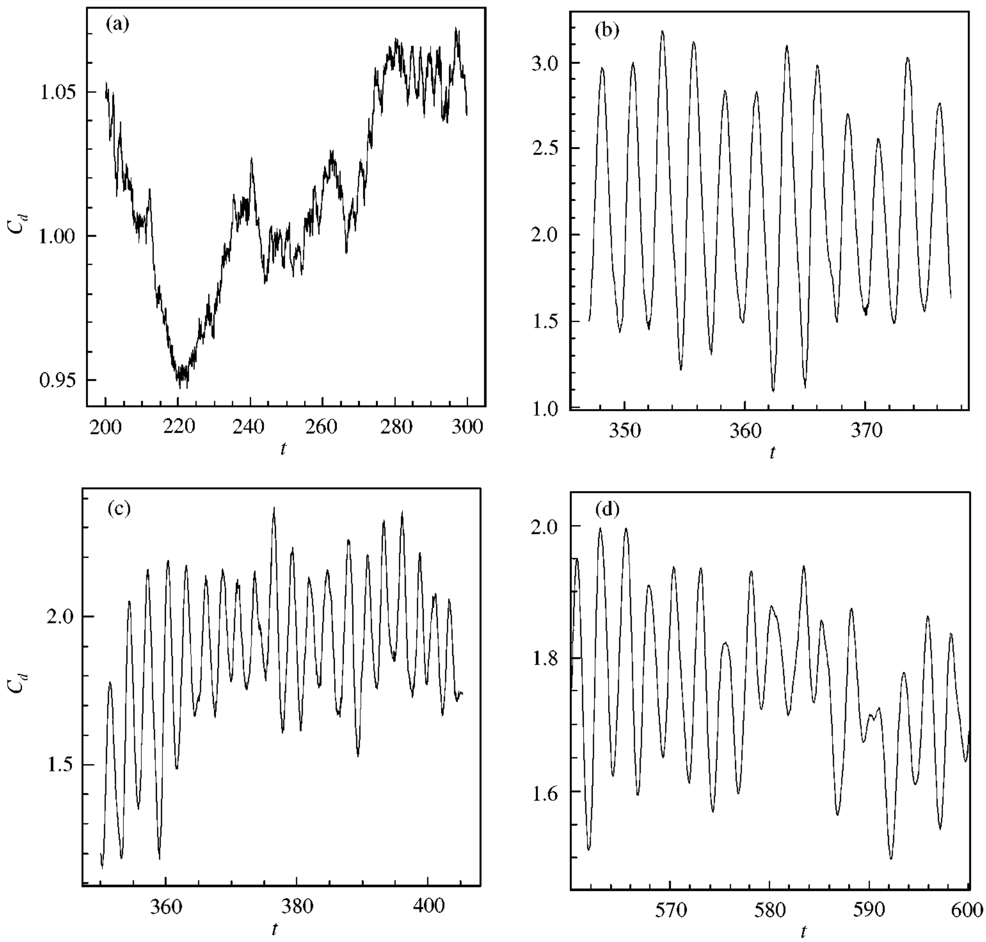

Figure 12. Comparison of span-averaged drag coefficient histories for (a) a stationary cylinder, (b) a freely oscillating rigid cylinder, (c) a short beam with free ends, and (d) a long beam with free ends.

the equation used for an oscillating rigid cylinder. For the DNS data presented here, if we take $A \approx 1$ and also $B = 1$ (with C_{d1} the stationary cylinder value) we obtain a value for C_d very close to the mean drag coefficient for a rigid cylinder as predicted by DNS. Finally, one can improve the formula in equation (8) by fitting the data as best as possible and select appropriate coefficients A and B. For example with $A = 0{\cdot}29$ and $B = 1{\cdot}79$ we obtain the curve marked with squares in Figure 13. However, this formula does not exhibit a decreasing slope for C_d with increasing amplitude (this remark was made by an anonymous referee). In summary, the often-used formula of Skop *et al.* in engineering analysis seems to overpredict the standing wave responses, which are more typical in ocean engineering applications.

5. SUMMARY AND DISCUSSION

In this paper we analyzed DNS data of flow past rigid and flexible cylinders subject to lock-in vortex-induced vibrations. We chose to perform all simulations at Re = 1000, as this corresponds to an order of magnitude increase compared to our previous studies Newman & Karniadakis (1997), while the corresponding flow exhibits a turbulent wake. Specifically,

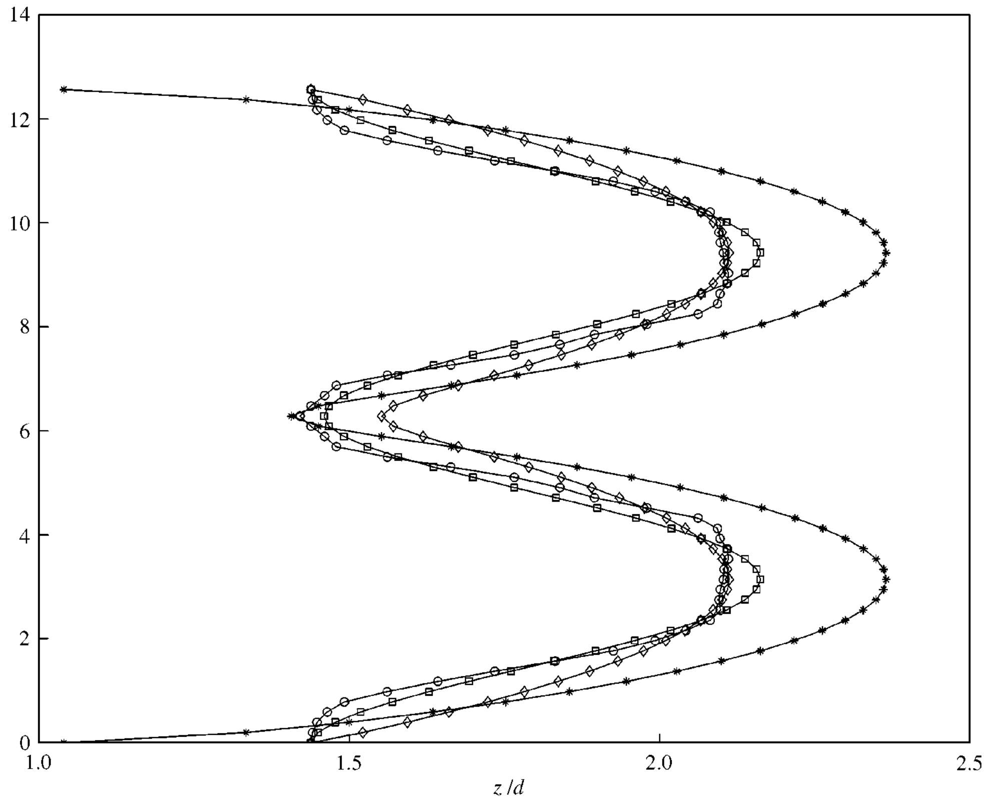

Figure 13. Mean drag coefficient along the beam for a short beam. Circles denote DNS data, stars denote the prediction by equation (7), squares denote the prediction by equation (8) for $A = 0{\cdot}29$ and $B = 1{\cdot}79$, and diamonds denote the prediction by equation (8) for $A = 0{\cdot}355$ and $B = 0{\cdot}9$.

TABLE 1

Summary of time- and span-averaged amplitude, lift and drag coefficients at lock-in. (zero structural damping is assumed and Re = 1000).

	y_{max}/d	$y_{r.m.s.}/d$	$(C_l)_{r.m.s.}$	C_d	$(C_d)_{r.m.s.}$
Stationary	0	0	0·12	1·04	0·02
Rigid	0·75	0·51	1·53	2·11	0·65
Short beam—Free	0·93	0·51	0·83	1·86	0·48
Short beam—Fixed	1·09	0·43	0·86	1·81	0·43
Long beam—Free	0·61	0·36	0·93	1·75	0·51
Long beam—Fixed	0·85	0·25	1·16	1·62	0·44

we presented results for two different responses of the cylinder motion, the first resembling a traveling (progressive) wave, and the second resembling a standing wave. The maximum cylinder displacement is about $0{\cdot}9d$ in the traveling wave case and $1{\cdot}1d$ in the standing wave case. The lift coefficient (r.m.s.) is about 0·8 for both cases but slightly larger for the standing wave. Similarly, the drag coefficient is about the same for both cases ($C_d \approx 1{\cdot}8$) but slightly lower for the standing wave. Detailed force distributions along the span and in time are given in the paper, and a summary of time- and span-averaged quantities is presented in Table 1.

The main assumption is that there is no structural damping in the system and that we operate at lock-in. As the Reynolds number is still relatively low compared to most experimental conditions, we expect some Reynolds number effects for the quantities summarized in Table 1. Other possible sources of error are: boundary conditions due to truncation of the domain, spatial and temporal discretization (primarily for the long-beam simulations), and time-averaging errors (due to low-frequency modulations). Based on various tests for all these factors [see, for example, Evangelinos (1999)], we expect the total error due to such sources to be less than 10%, and thus the results in Table 1 are accurate within that range.

We also tested the applicability of the often-used formula for predicting the drag coefficient based on the standard deviation of the motion Skop *et al.* (1977), and we found it to overpredict the calculated values. A similar model we proposed but with very different coefficients seemed to fit the data better. On the other hand, DNS studies of the type presented here are currently prohibitively expensive to be used in engineering design of VIV. The question then remains, as to what will be a good and efficient model to predict mean forces or force distribution in VIV applications. We believe that the answer could be provided by dynamical systems modeling, given the low dimensionality of the wake.

To test this hypothesis, we have repeated the DNS for case A_s (short beam with periodic ends) but with significantly reduced resolution, i.e., we reduced the number of degrees of freedom (d.o.f.) from about 5 millions per field in the previous simulations to approximately 50 000 d.o.f. per field, with only two complex Fourier modes (i.e., four physical planes) along the span of $4\pi d$. The response is shown in Figure 14 where we plot the amplitude of the motion along the span and in time. We see that a standing wave response is obtained with somewhat reduced amplitude compared to the high-resolution simulation. The corresponding mean drag coefficient is $C_d \approx 2{\cdot}0$, which is about 10% higher than in the high-resolution simulation but approximately 15% lower than the corresponding two-dimensional simulation. We recall here that with only two (complex) Fourier modes along the span, we resolve basically the mean flow (with the zeroth mode) and the first excited mode. In other words, we resolve only one three-dimensional mode, which apparently is sufficient to give a big improvement (compared to the two-dimensional predictions) in the force distribution and also the motion amplitude, given that the maximum amplitude of the two-dimensional simulation is only $0{\cdot}55d$. We also note that the Fourier representation along the span is the best possible representation from the approximation point of view. However, there was no attempt here to obtain the best representation of the flow by constructing an appropriate hierarchy of the most energetic modes in the planes perpendicular to the cylinder axis, using for example the Karhunen-Loève approach (Newman & Karniadakis 1996). We expect that this more systematic approach will result in a substantially lower-dimensional representation to predict the dynamics of VIV. We are currently working on that front and we will report results in the near future.

ACKNOWLEDGMENTS

This work was supported by the Office of Naval Research (Dr T.F. Swean) and the Department of Energy (Dr F. Howes). Computations were performed on the T3E at NAVO and on the SP2 at Maui High Performance Computing Center. We would also like to thank Dr Gunnar Furnes of Norsk Hydro, Norway, for very useful discussions.

REFERENCES

ALEXANDER, C. 1981 The complex vibrations and implied drag of a long oceanographic wire in crossflow. *Ocean Engineering* **8,** 379–406.

BLEVINS, R. 1990 *Flow Induced Vibration*. New York: Van Nostrand Reinhold.

BLOOR, M. 1964 The transition to turbulence in the wake of a circular cylinder. *Journal of Fluid Mechanics* **19,** 290.

BRIKA, D. & LANEVILLE, A. 1993 Vortex-induced vibrations of a long flexible circular cylinder. *Journal of Fluid Mechanics* **250,** 481–508.

EVANGELINOS, C. 1999 Parallel simulations of vortex-induced vibrations in turbulent flow: linear and non-linear models. Ph.D. thesis, Division of Applied Mathematics, Brown University.

EVANGELINOS, C. & KARNIADAKIS, G. 1999 Dynamics and flow structures in the turbulent wake of rigid and flexible cylinders subject to vortex-induced vibrations. *Journal of Fluid Mechanics* **400**, 91.

FENG, C. 1968 The measurement of vortex-induced effects in flow past a stationary and oscillating circular and D-section cylinders. Master's Thesis, University of British Columbia, Vancouver, B.C., Canada.

FURNES, G. 1998 On marine riser responses in time and depth dependent flows. Technical Report, Norsk Hydro, Bergen, Norway.

GOPALKRISHNAN, R. 1993 Vortex-induced forces on oscillating bluff cylinders. Ph.D. Thesis, Department of Ocean Engineering, MIT, Cambridge, MA, U.S.A.

HOVER, F., TECHET A. & TRIANTAFYLLOU, M. 1998 Forces on oscillating uniform and tapered cylinders in crossflow. *Journal of Fluid Mechanics* **363,** 97–114.

KHALAK, A. & WILLIAMSON, C. 1996 Dynamics of a hydroelastic cylinder with very low mass and damping. *Journal of Fluids and Structures* **10,** 455–472.

KHALAK, A. & WILLIAMSON, C. 1997 Fluid forces and dynamics of a hydroelastic structure with very low mass and damping. *Journal of Fluids and Structures* **11,** 973–982.

KIM, Y.-H., VANDIVER, J. & HOLLER, R. 1985 Vortex-induced vibration and drag coefficients of long cables subjected to sheared flows. In *Proceedings of the Fourth International Offshore Mechanics and Arctic Engineering Symposium*, New York ASME.

NAUDASCHER, E. & ROCKWELL, D. 1993 *Flow-Induced Vibrations. An Engineering Guide*. Rotterdam: A.A. Balkema.

NEWMAN, D. & KARNIADAKIS, G. 1996 Low-dimensional modeling of flow-induced vibrations via proper orthogonal decomposition. In *Proceedings of the 21st Symposium on Naval Hydrodynamics*, Norway, pp. 605–621.

NEWMAN, D. & KARNIADAKIS, G. 1997 Simulations of flow past a freely vibrating cable. *Journal of Fluid Mechanics* **344,** 95–136.

PARKINSON, G. 1989 Phenomena and modeling of flow-induced vibrations of bluff bodies. *Progress in Aerospace Science* **26,** 169–224.

SARPKAYA, T. 1978 Fluid forces on oscillating cylinders. *ASCE Journal of Waterway, Port, Coastal, and Ocean Division* **104,** 275–290.

SKOP, R., GRIFFIN, O. & RAMBERG, S. 1977 Strumming predictions for the SEA-CON II experimental mooring. *Offshore Technology Conference*, Paper OTC 2884.

STAUBLI, T. 1983 Calculation of the vibration of an elastically-mounted cylinder using experimental data from forced oscillation. *ASME Journal of Fluids Engineering* **105,** 225–229.

VANDIVER, J. 1983 Drag coefficients for long, flexible cylinders. *Offshore Technology Conference*, Paper OTC 4490.

WARBURTON, T. 1998 Spectral/hp element methods on polymorphic multi-domains: Algorithms and applications. Ph.D. Thesis, Division of Applied Mathematics, Brown University.

WARBURTON, T. & KARNIADAKIS, G. 1997 Spectral simulation of flow past a cylinder close to a free surface. In *FEDSM97-3689*, *Proceedings of Fluids Engineering Division Summer Meeting*, Vancouver, B.C., Canada.

YOERGER, D., GROSENBAUGH, M., TRIANTAFYLLOU, M. & BURGESS, J. 1991 Drag forces and flow-induced vibrations of a long vertical tow cable—Part 1: Steady-state towing conditions. *Journal of Offshore Mechanics and Arctic Engineering* **113,** 117–127.

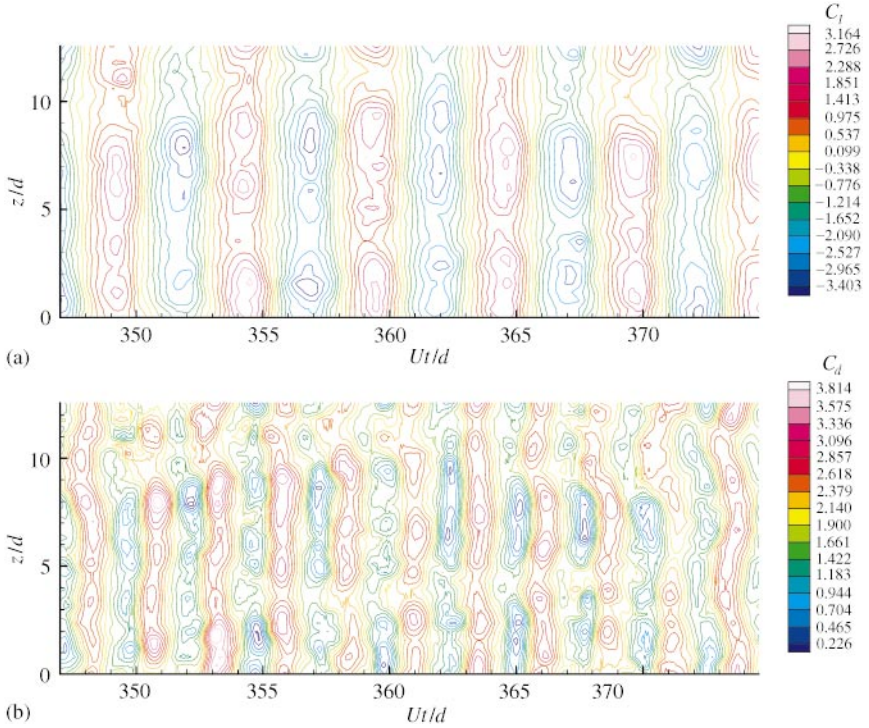

Figure 2. Rigid cylinder: (a) lift coefficient along the span versus time; (b) drag coefficient along the span versus time.

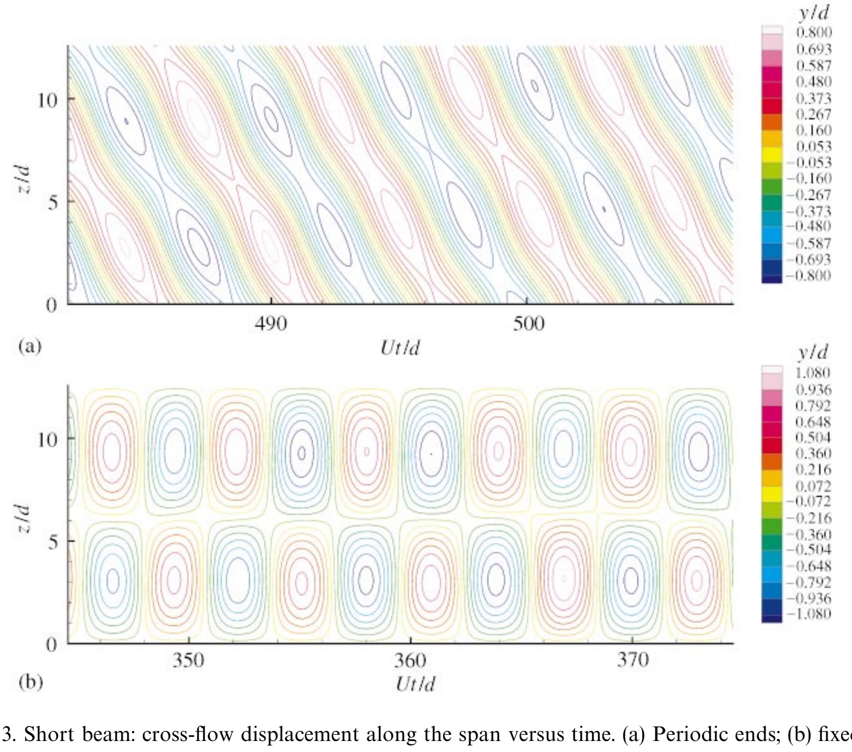

Figure 3. Short beam: cross-flow displacement along the span versus time. (a) Periodic ends; (b) fixed ends.

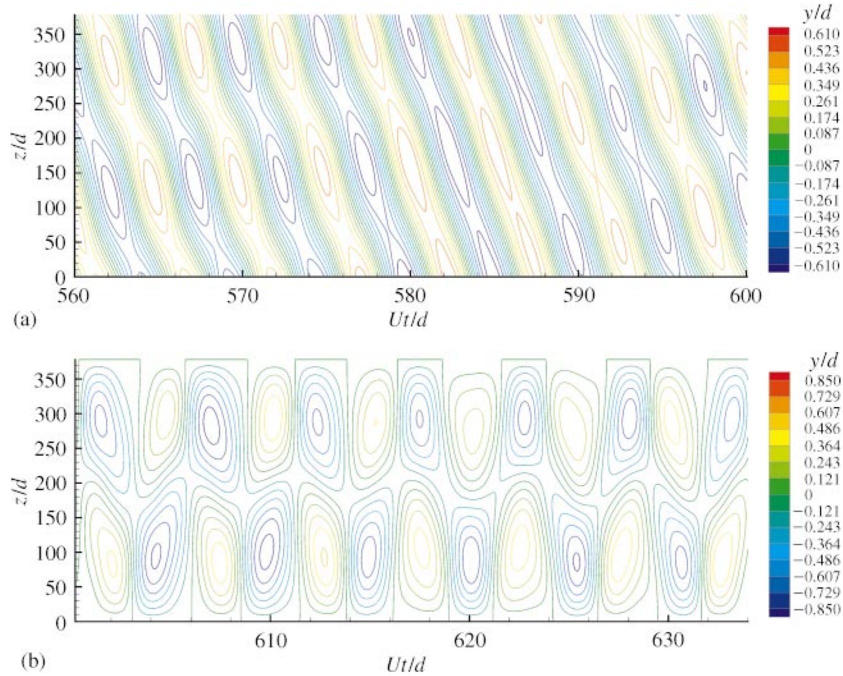

Figure 4. Long beam: cross-flow displacement along the span versus time. (a) Periodic ends; (b) fixed ends.

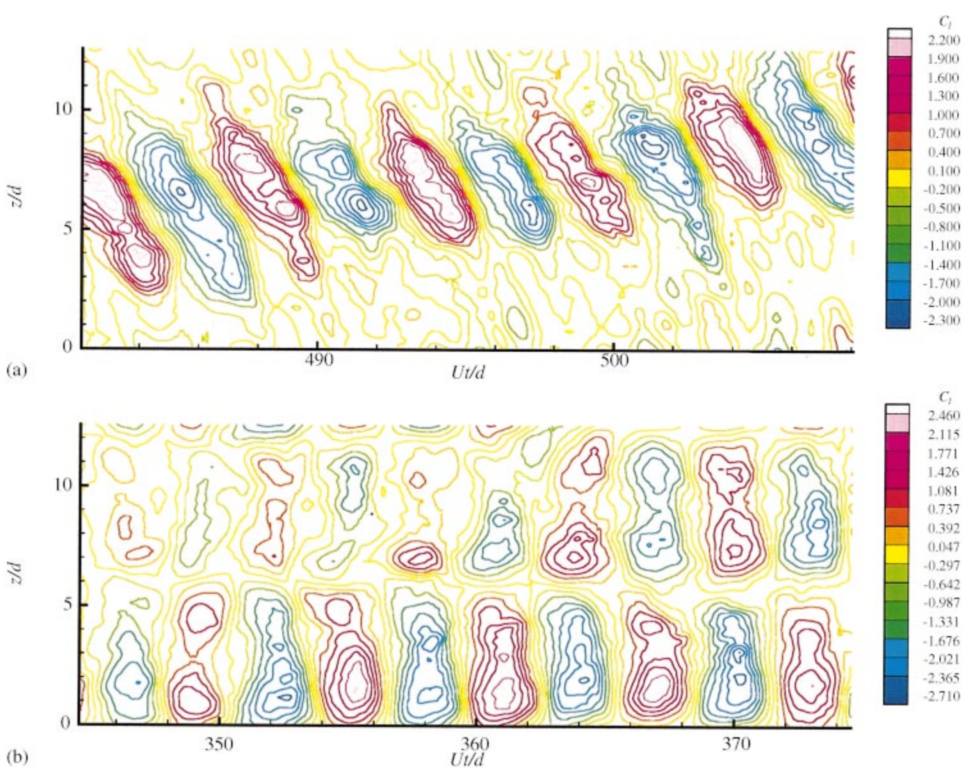

Figure 5. Short beam: lift coefficient along the span versus time. (a) Periodic ends; (b) fixed ends.

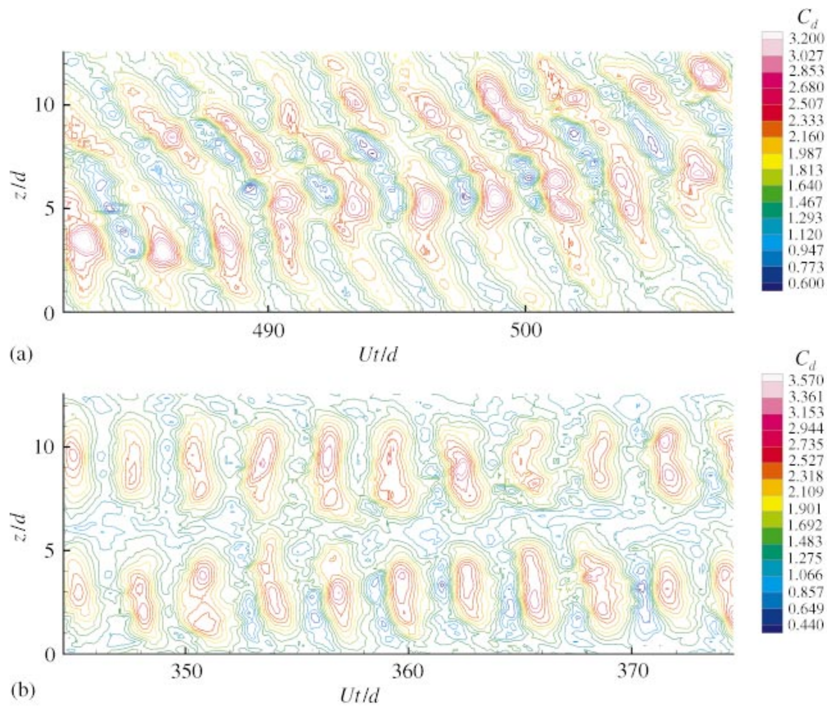

Figure 6. Short beam: drag coefficient along the span versus time. (a) Periodic ends; (b) fixed ends.

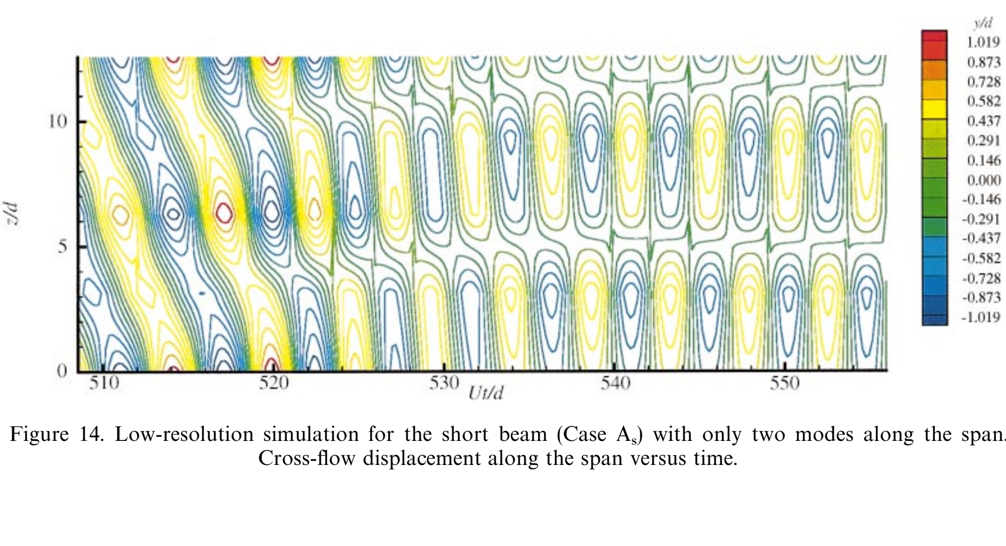

Figure 14. Low-resolution simulation for the short beam (Case A_s) with only two modes along the span. Cross-flow displacement along the span versus time.